Intranasal Immunization with a Lentiviral Vector Coding for SARS-CoV-2 Spike Protein Confers Vigorous Protection in Pre-Clinical Animal Models

Abstract

We developed a potent vaccination strategy, based on lentiviral vector (LV), capable of inducing neutralizing antibodies specific to the Spike glycoprotein (S) of SARS-CoV-2, the etiologic agent of CoronaVirus Disease 2019 (COVID-19). Among several LV encoding distinct variants of S, a single one encoding the full-length, membrane anchored S (LV::S_{FL}) triggered high antibody titers in mice, with neutralization activities comparable to patients recovered from COVID-19. LV::S_{FL} systemic vaccination in mice, in which the expression of the CoV2 receptor hACE2 was induced by transduction of the respiratory tract cells by an adenoviral type 5 (Ad5) vector, despite an intense serum neutralizing activity, only ≈1 $\log_{10}$ reduction of lung viral loads was observed after SARS-CoV2 challenge.

We thus explored the strategy of targeting the immune response to the upper respiratory tract through an intranasal boost administration. Even though, after a prime and target regimen, the systemic neutralizing activity did not increase substantially, ≈5 $\log_{10}$ decrease in lung viral loads was achieved, with the loads in some animals under the limit of detection of a highly sensitive RT-PCR assay. The conferred protection also avoided largely pulmonary inflammation. We confirmed the vaccine efficacy and inhibition of lung inflammation using both integrative and non-integrative LV platforms in golden hamsters, naturally permissive to SARS-CoV2 replication and restituting human COVID-19 physiopathology. Our results provide the proof-of-principle evidence of marked prophylactic effects of an LV-based vaccination strategy against SARS-CoV-2 in two pre-clinical animal models and designate the intranasal LV::S_{FL}-based immunization as a vigorous and promising vaccine approach against COVID-19.

Intranasal Immunization with a Lentiviral Vector Coding for SARS-CoV-2 Spike Protein Confers Vigorous Protection in Pre-Clinical Animal Models

Min-Wen Ku[1*], Maryline Bourgine[1,2*], Pierre Authié[1*], Jodie Lopez[1], Kirill Nemirov[1], Fanny Moncoq[1], Amandine Noirat[1], Benjamin Vesin[1], Fabien Nevo[1], Catherine Blanc[1], Philippe Souque[2], Emeline Simon[3], Houda Tabbal[3], Hugo Mouquet[4], François Anna[1], Annette Martin[3], Nicolas Escriou[5], Laleh Majlessi[1£] and Pierre Charneau[1,2£]

[1]Institut Pasteur-TheraVectys Joint Lab, 28 rue du Dr. Roux, Paris F-75015, France

[2]Molecular Virology and Vaccinology Unit, Institut Pasteur

[3]Molecular Genetics of RNA Viruses Unit, Institut Pasteur. CNRS UMR3569, Université Paris Diderot-Sorbonne, Paris Cité, Paris, France

[4]Laboratory of Humoral Immunology, Institut Pasteur, INSERM U1222

[5]Innovation Lab, Vaccines, Institut Pasteur

[*]Equal contribution of the authors

[£]Co-senior and co-corresponding authors

Abstract

We developed a potent vaccination strategy, based on lentiviral vector (LV), capable of inducing neutralizing antibodies specific to the Spike glycoprotein (S) of SARS-CoV-2, the etiologic agent of CoronaVirus Disease 2019 (COVID-19). Among several LV encoding distinct variants of S, a single one encoding the full-length, membrane anchored S (LV::S_{FL}) triggered high antibody titers in mice, with neutralization activities comparable to patients recovered from COVID-19. LV::S_{FL} systemic vaccination in mice, in which the expression of the CoV2 receptor hACE2 was induced by transduction of the respiratory tract cells by an adenoviral type 5 (Ad5) vector, despite an intense serum neutralizing activity, only ≈1 $\log_{10}$ reduction of lung viral loads was observed after SARS-CoV2 challenge.

We thus explored the strategy of targeting the immune response to the upper respiratory tract through an intranasal boost administration. Even though, after a prime and target regimen, the systemic neutralizing activity did not increase substantially, ≈5 $\log_{10}$ decrease in lung viral loads was achieved, with the loads in some animals under the limit of detection of a highly sensitive RT-PCR assay. The conferred protection also avoided largely pulmonary inflammation.

We confirmed the vaccine efficacy and inhibition of lung inflammation using both integrative and non-integrative LV platforms in golden hamsters, naturally permissive to SARS-CoV2 replication and restituting human COVID-19 physiopathology. Our results provide the proof-of-principle evidence of marked prophylactic effects of an LV-based vaccination strategy against SARS-CoV-2 in two pre-clinical animal models and designate the intranasal LV::S_{FL}-based immunization as a vigorous and promising vaccine approach against COVID-19.

Introduction

The new Severe Acute Respiratory Syndrome beta-coronavirus 2 (SARS-CoV-2) that emerged in late 2019 in Wuhan, China, is extraordinarily contagious and fast-spreading across the world (Guo et al., 2020). Compared to the previously emerged SARS or Middle East Respiratory Syndrome (MERS) coronaviruses, SARS-CoV-2 causes unprecedented threat on global health and tremendous socio-economic consequences. Therefore, the development of effective prophylactic vaccines against SARS-CoV-2 is an absolute imperative to contain the spread of the epidemic and to attenuate the onset of CoronaVirus Disease 2019 (COVID-19), such as deleterious inflammation and progressive respiratory failure (Amanat and Krammer, 2020).

Coronaviruses are enveloped, non-segmented positive-stranded RNA viruses, characterized by their envelope-anchored Spike (S) glycoprotein (Walls et al., 2020). The SARS-CoV-2 S (S_{CoV-2}) is a $(180\ kDa)_3$ homotrimeric class I viral fusion protein, that engages the carboxypeptidase Angiotensin-Converting Enzyme 2 (ACE2), expressed on host cells. The monomer of S_{CoV-2} protein possesses an ecto-domain, a transmembrane anchor domain, and a short internal tail. S_{CoV-2} is activated by a two-step sequential proteolytic cleavage to initiate fusion with the host cell membrane. Subsequent to S_{CoV-2}-ACE2 interaction, through a conformational reorganization, the extracellular domain of S_{CoV-2} is first cleaved at the highly specific furin $682^{RRAR}685$ site (Guo et al., 2020; Walls et al., 2020), a key factor determining the pathological features of the virus, linked to the ubiquitous furin expression (Wang et al., 2020). The resulted subunits are constituted of: (i) S1, which harbors the ACE2 Receptor Binding Domain (RBD), with the atomic contacts restricted to the ACE2 protease domain, and (ii) S2, which bears the membrane-fusion elements. Like for S_{CoV-1}, the shedding of S1 renders accessible on S2 the second proteolytic cleavage site 797^{R}, namely S2' (Belouzard et al., 2009). According to the cell or tissue types, one or several host proteases, including furin, trypsin, cathepsins or transmembrane protease serine protease-2 or -4, can be involved in this second cleavage step (Coutard et al., 2020). The consequent "fusogenic" conformational changes of S lead to the exposure of a Fusion Peptide (FP), adjacent to S2'. Insertion of FP to the host cell/vesicle membrane primes the fusion reaction, whereby the viral RNA release into the host cytosol (Lai et al., 2017). The facts that the S_{CoV-2}-ACE2 interaction is the only mechanism, thus far identified for the host cell infection by SARS-CoV-2, and that the RBD contains numerous conformational B-cell epitopes (Walls et al., 2020), designate this viral envelope glycoprotein as the main target for neutralizing antibodies (nAbs).

Compared to: (i) attenuated or inactivated viral vaccine candidates which require extensive safety testing, (ii) nucleic acid encoding for S without proven efficacy, (iii) protein vaccines which require the use of adjuvants and boosting, viral vector vaccines, such as adenoviral vectors, can generate strong immune response. However, adenoviral vectors are target of pre-existing immunity in the human population, which largely reduces their immunogenicity (Rosenberg et al., 1998; Schirmbeck et al.,

2008). Non-replicative lentiviral vaccinal vectors (LV) possess a large potential at eliciting strong and long-lasting adaptive immunity, including Ab responses (Di Nunzio et al., 2012; Hu et al., 2011; Ku et al., 2020; Zennou et al., 2000). The safety of these vectors has been demonstrated in human in a phase 1 HIV-1 vaccine trial (2011-006260-52 EN). In addition, LV are majorly pseudo-typed with Vesicular Stomatitis Virus envelope Glycoprotein (VSV-G), with negligible exposure in human population, which minimizes the risk of vaccine efficacy reduction linked to a pre-existing cross-reactive immunity as described for other viral vectors (Hu et al., 2011).

To develop a vaccine candidate able to induce nAbs specific to S_{CoV-2}, we generated LV coding for: (i) full-length, membrane anchored form of S (LV::S_{FL}), (ii) S1-S2 ecto-domain, without the transmembrane and internal tail domains (LV::S1-S2), or (iii) S1 alone (LV::S1). We established that LV::S_{FL} gave rise to elevated amounts of nAbs, inhibiting the $ACE2^+$ host-cell invasion by S_{CoV-2}-pseudo-typed virions. S_{CoV-2}-specific T cells were also efficaciously induced in LV::S_{FL}-immunized animals. Moreover, in a mouse model in which the expression of human ACE2 (hACE2) was induced in the respiratory tracts by an adenoviral vector serotype 5 (Ad5), as well as in golden hamsters, we demonstrated a strong prophylactic effect of LV::S_{FL} immunization against the replication of a SARS-CoV-2 clinical isolate, accompanied by the reduction of infection-related inflammation in the lungs. Importantly, boost/target immunization with LV::S_{FL} via nasal route was instrumental in the protection efficacy. Our virological and immunological criteria provided the proof-of-principle evidence of: (i) marked prophylactic effects of a viral vector-based vaccination strategy against SARS-CoV-2, (ii) the fact that LV-based immunization represents a promising strategy to develop vaccine candidates against coronaviruses, and (iii) requirement of mucosal immunization to reach vigorous protective lung immunity.

Results

Induction of antibody responses by LV encoding SARS-CoV-2 Spike protein variants

To develop a vaccine candidate able to induce nAbs specific to S_{CoV-2}, we generated LV coding, under the transcriptional control of the cytomegalovirus (CMV) immediate-early promoter, for codon-optimized sequences of: (i) full-length, membrane anchored form of S (LV::S_{FL}), (ii) S1-S2 ecto-domain, without the transmembrane and C-terminal short internal tail (LV::S1-S2), or (iii) S1 alone (LV::S1), which all harbor the RBD **(Figure 1A, Supplemental Figure 1)**, with prospective conformational heterogeneities. To evaluate the humoral responses induced by these vectors, C57BL/6 mice (n = 4/group) were immunized by a single i.p. injection of 1×10^7 TU/mouse of either LV, or an LV encoding GFP as negative control. S_{CoV-2}-specific Ab responses were investigated in the sera at weeks 1, 2, 3, 4 and 6 post immunization **(Figure 1B)**. In LV::S_{FL} or LV::S1-S2-immunized mice, S_{CoV-2}-specific immunoglobulin G (IgG) were detectable as early as 1 week post immunization and their amounts exhibited a progressive increment until week 6 post immunization with Mean titer ± SEM of $(4.5 \pm 2.9) \times 10^6$ or $(1.5 \pm 1) \times 10^6$, respectively. In comparison, S_{CoV-2}-specific IgG titers were 100× lower, i.e., $(7.1 \pm 6.1) \times 10^4$, in their LV::S1-immunized counterparts.

Sera were then evaluated for their capacity to neutralize SARS-CoV-2, using a reliable neutralization assay based on nAb-mediated inhibition of $hACE2^+$ cell invasion by non-replicative LV particle surrogates, pseudo-typed with S_{CoV-2} (Sterlin et al.). Such S_{CoV-2} pseudo-typed LV particles, harbor the reporter luciferase gene, which allows quantitation of the $hACE2^+$ host cell invasion, inversely proportional to the neutralization efficiency of nAbs possibly contained in the biological fluids. Analysis of 50% Effective Concentrations (EC50) of the sera from the LV::S_{FL}-, LV::S1-S2- or LV::S1-immunized mice clearly established that LV::S_{FL} was the most potent vector at inducing S_{CoV-2}-specific nAbs **(Figure 1C)**. Moreover, nAb titers were correlated with S_{CoV-2}-specific IgG titers only in the sera of LV::S_{FL}-immunized mice ($p < 0.0001$, $R^2 = 0.645$, two-sided Spearman rank-correlation test) **(Figure 1D)**. These results strongly suggest that in the S1-S2 or S1 polypeptides, the conformations of pertinent B-cell epitopes are distinct from those of the native S_{FL}, the latter representing the only variant which induces nAbs able to inhibit the S_{CoV-2}-hACE2 interaction and host cell invasion. Comparison of the neutralizing capacity of sera from the LV::S_{FL}-immunized mice and a cohort of mildly symptomatic infected people living in Crépy en Valois, one of the first epidemic zones appeared in France, showed equivalent neutralizing activity average **(Figure 1E)**. These data predict a potentially protective humoral response induced by LV::S_{FL}.

LV::S_{FL}-immunized C57BL/6 mice also displayed S_{CoV-2}-specific T-cell responses, as detected at week 2 post-immunization by IFNγ ELISPOT assay following stimulation with distinct pools of S_{CoV-2}-derived 15-mer peptides, spanning the S_{FL} **(Figure 2A)**. Significant amounts of responding T cells were detected for 4 out of 10 peptide pools. Deconvolution of the 4 positive pools by intracellular

cytokine staining detected at least one immunogenic region able to stimulate $CD4^+$ T cells (**Figure 2B,** right panel) versus 4 regions able to stimulate $CD8^+$ T cells (**Figure 2B,** left panel), which is in accordance with the favored orientation of LV-encoded antigens to the MHC-I presentation pathway (Hu et al., 2011).

Set up of a murine model expressing human ACE2 in the respiratory tracts

As S_{CoV-2} does not interact well with murine ACE2, wild-type laboratory mice are not permissive to replication of SARS-CoV-2 clinical isolates. Due to unavailability of hACE2 transgenic mice in Europe during the progression of the present study, we sought to elaborate a murine model in which the hACE2 expression is induced in the respiratory tracts and pulmonary mucosa to evaluate the LV::S_{FL} vaccine efficacy. We generated an Ad5 gene delivery vector able to vehicle in non-integrating episomes, the gene coding for hACE2 under the transcriptional control of CMV promoter (Ad5::hACE2). We first checked in vitro the potential of the Ad5::hACE2 vector to transduce HEK293T cells by RT-PCR **(Figure 3A)**. To achieve in vivo transduction of respiratory tract cells, we instilled i.n. 2.5×10^9 IGU/mouse of Ad5::hACE2 into C57BL/6 mice. Four days later, the hACE2 protein expression was detectable in the lung cell homogenate by Western Blot **(Figure 3B)**. To get more insights into the in vivo expression profile of a transgene administered under these conditions, we instilled i.n. the same dose of an Ad5::GFP reporter vector into C57BL/6 mice. As evaluated by flow cytometry, 4 days post instillation, the GFP reporter was expressed not only in the lung epithelial $EpCam^+$ cells, but also in lung immune cells, as tracked by CD45 pan-hematopoietic marker **(Figure 3C)**, showing that this approach allows efficient transduction of epithelial cells which however is not restricted to these cells.

To evaluate the permissibility of such hACE2-transduced mice to SARS-CoV-2 infection, 4 days after i.n. pretreatment with either Ad5::hACE2 or an empty control Ad5 vector, C57BL/6 mice were inoculated i.n. with 1×10^5 $TCID_{50}$ of a SARS-CoV-2 clinical isolate, which was isolated in February 2020 from a COVID-19 patient by the National Reference Centre for Respiratory Viruses (Institut Pasteur, France). The lung viral loads, determined at 2 days post inoculation (dpi), were as high as $(4.4 \pm 1.8) \times 10^9$ copies of SARS-CoV-2 RNA/mouse in Ad5::hACE2-pretreated mice, compared to only $(6.2 \pm 0.5) \times 10^5$ copies/mouse in empty Ad5-pretreated, or $(4.0 \pm 2.9) \times 10^5$ copies/mouse in un-pretreated mice **(Figure 3D)**. At 4 dpi, the lung viral loads were maintained in Ad5::hACE2-pretreated mice $(2.8 \pm 1.3 \times 10^9$ copies/mouse), whereas a drop to $(1.7 \pm 2.3) \times 10^4$ or $(3.9 \pm 5.1) \times 10^3$ copies/mouse was observed in empty Ad5-pretreated or unpretreated mice, respectively. At 7 dpi, in Ad5::hACE2-pretreated mice, the viral loads decreased significantly, albeit were still largely detectable $((1.33 \pm 0.9) \times 10^6$ copies/mouse).

Ad5::hACE-2 i.n. instillation induced $CD45^+$ cell recruitment to the lungs **(Figure 3E)**. However, this effect was reduced with decreasing vector doses, as determined at day 4 post instillation. The dose

of 4×10^8 IGU/mouse did not cause $CD45^+$ cell recruitment, as compared to the PBS-treated controls, but still conferred full permissibility to SARS-CoV-2 replication **(Figure 3F)**. The permissibility of Ad5-hACE2-pretreated mice to SARS-CoV-2 replication and the set-up of this model paved the way for the in vivo assessment of vaccine or drug efficacy against SARS-CoV-2 in mice.

Evaluation of the protective potential of LV::S_{FL} against SARS-CoV-2 in mice

To investigate the prophylactic potential of LV::S_{FL} against SARS-CoV-2, C57BL/6 mice (*n* = 4/group) were injected i.p. with a single dose of 1×10^7 TU/mouse of LV::S_{FL} or a negative control LV (sham). At week 7 post immunization, mice were pretreated with Ad5::hACE2, and 4 days later, inoculated i.n. with 1×10^5 $TCID_{50}$ of SARS-CoV-2 **(Figure 4A)**. At 3 dpi, the lung viral loads in LV::S_{FL}-vaccinated mice was reduced by ~1 log_{10}, i.e., Mean ± SEM of $(3.2 \pm 2.2) \times 10^8$ SARS-CoV-2 RNA copies/mouse compared to $(1.7 \pm 0.9) \times 10^9$ or $(2.4 \pm 1.6) \times 10^9$ copies/mouse in the un- or sham-vaccinated mice, respectively **(Figure 4B)**. Therefore, a single LV::S_{FL} injection effectively afforded ~90% inhibition of the viral replication in the lungs.

To further improve the prophylactic effect, we evaluated the prime-boost or prime-target approaches. C57BL/6 mice (*n* = 4-5/group) were primed i.p. with 1×10^7 TU/mouse of LV::S_{FL} or a control LV at week 0, and then boosted at week 3 with: (i) 1×10^7 TU/mouse of the same LV via i.p. ("LV::S_{FL} i.p-i.p.", prime-boost), or (ii) with 3×10^7 TU/mouse via i.n. ("LV::S_{FL} i.p.-i.n.", prime-target) to attract the mediators of systemic immunity to the lung mucosa **(Figure 4C)**. The sera were investigated after boost/target. Systemic boosting with LV::S_{FL} via i.p. resulted in a significant increase in the anti-S_{CoV-2} IgG titers, which was more obvious when the binding was evaluated against the full length S **(Figure 4D, left)**, compared to S1 or RBD fragment alone **(Supplemental Figure 2)**. This observation may suggest that the concerned B-cell epitopes could be of conformational type. In contrast, mucosal targeting with LV::S_{FL} via i.n. did not lead to a statistically significant improvement of anti-S_{CoV-2} IgG titers at the systemic level **(Figure 4D left, Supplemental Figure 2)**. In terms of serum neutralization potential, even though a trend to increase was observed after i.p. or i.n. boost, the differences did not reach statistical significance **(Figure 4D right)**.

All the mice were then pretreated with Ad5::hACE2 and challenged with 0.3×10^5 $TCID_{50}$ of SARS-CoV-2 at week 4. At 3 dpi, the lung viral loads were significantly lower in LV::S_{FL} i.p.-i.p. immunized mice than in sham-vaccinated mice, i.e., $(6.8 \pm 3.7) \times 10^8$ vs $(1.1 \pm 1.6) \times 10^8$ copies of SARS-CoV-2 RNA/mouse, respectively **(Figure 4F)**. This viral load reduction was similar to that obtained with a single LV::S_{FL} administration **(Figure 4B)**. However, most importantly, after i.n. LV::S_{FL} target immunization, a sharp decrease of up to 4 log_{10} was observed in the viral loads compared to the sham-vaccinated group, and 2 out of 5 mice achieved undetectable viral RNA in the lungs. Therefore, increasing the nAb titers at the systemic levels does not necessarily improve the SARS-CoV-2-specific

protection, but a mucosal i.n. target immunization, which attracts the immune effectors to the site of the potential viral infection, contributes substantially to the inhibition of SARS-CoV-2 replication.

Based on the compelling evidence of innate immune hyperactivity in the acute lung injury in COVID-19 (Vabret et al., 2020), we investigated the possible variations of the lung innate immune cell subsets **(Figure 5A)**, in the non-infected controls, sham-vaccinated or LV::S_{FL}-vaccinated mice inoculated with SARS-CoV-2. At 3 dpi, we detected no differences in the proportions of basophils or NK cells versus total lung $CD45^+$ cells among the experimental groups **(Figure 5B)**. In net contrast, we detected increased proportions of alveolar macrophages, dendritic cells, mast cells, eosinophils, $Ly6C^+$ or $Ly6C^-$ monocytes/macrophages or neutrophils versus total lung $CD45^+$ cells, in sham-vaccinated mice which displayed the highest lung viral loads. These observations demonstrate that in this mouse model, the increased lung SARS-CoV-2 loads are correlated with the recruitment of several inflammation-related innate immune cells, and that vaccine-mediated anti-viral protection dampens or avoids such inflammation. This was corroborated with the reduced cytokine and chemokine contents in the lungs of mice vaccinated by prime-boost/target with LV::S_{FL}, as evaluated by qRT-PCR applied to RNA extracted from the total lung homogenates **(Figure 5C)**. Therefore, the conferred protection also avoided pulmonary inflammation linked to SARS-CoV-2 infection.

Evaluation of the protective potential of LV::S_{FL} against SARS-CoV-2 in golden hamsters

Outbred *Mesocricetus auratus*, so-called golden hamsters, provide a suitable pre-clinical model to study the COVID-19 pathology, since the ACE2 ortholog of this species interacts efficaciously with S_{CoV-2}, whereby host cell invasion and viral replication (Sia et al., 2020). We thus investigated the prophylactic effect of LV::S_{FL} vaccination on SARS-CoV-2 infection in this pertinent model. Although integrative LV are largely safe and passed successfully a phase 1 clinical trial (2011-006260-52 EN), in addition to the LV::S_{FL}, we also evaluated an integrase deficient, non-integrative version of LV::$_{SFL}$ (NILV) with the prospect of application in future clinical trials.

To assess the prophylactic effect of vaccination following prime-boost/target regimen, *M. auratus* hamsters (n = 6/group) were: (i) primed i.p. with a low dose of 1×10^6 TU of LV::S_{FL} and boosted i.n. at week 5 with 4×10^7 TU of LV::S_{FL}, ("LV::S_{FL} i.p.-i.n. Low"), (ii) primed i.p. with a high dose of 1×10^7 TU of LV::S_{FL} and boosted i.n. at week 5 with 4×10^7 TU of LV::S_{FL} ("LV::S_{FL} i.p.-i.n. High"), or (iii) primed intramuscularly (i.m.) with 1×10^8 TU of NILV::S_{FL} and boosted i.n. at week 5 with the same dose of NILV::S_{FL} ("NILV::S_{FL} i.m.-i.n.") **(Figure 6A)**. Sham-vaccinated controls received the same amounts of an empty LV via i.p. and then i.n. routes. Strong and comparable S_{CoV-2}-specific IgG antibodies were detected by ELISA in the sera of hamsters from the three vaccinated groups, before and after the i.n. boost **(Figure 6B)**. Post boost/target serology detected neutralization activity in all the groups, with the highest EC50 average observed in "int LV::S_{FL} i.p.-i.n. High" individuals. Such levels were comparable to those detected in asymptomatic, pauci-symptomatic, symptomatic or healthy

COVID-19 contacts in humans **(Figure 6C)**. All the hamsters were challenged i.n. with 0.3×10^5 $TCID_{50}$ of SARS-CoV-2 at week 5. Up to 16% weight loss was progressively reached at 4 dpi in sham-vaccinated individuals, compared to non-significant loss in all the LV::S_{FL}-vaccinated groups **(Figure 6D)**.

At 2 dpi, decreases of ~1.5-to-3 log_{10} were observed in the lung viral loads of "int LV::S_{FL} i.p.-i.n. Low", "int LV::S_{FL} i.p.-i.n. High" and "non int LV::S_{FL} i.m.-i.n." groups, compared to sham-vaccinated hamsters **(Figure 7A)**. At 4 dpi, the magnitude of viral load reductions in the vaccinated groups were much more important and reached >4 log_{10}, compared to the sham-vaccinated individuals. As evaluated by qRT-PCR in the total lung homogenates of the protected "int LV::S_{FL} i.p.-i.n. Low", "int LV::S_{FL} i.p.-i.n. High" and "NILV::S_{FL} i.m.-i.n." groups, substantial decreases were observed in the expression of inflammatory cytokines, for instance IFNγ and IL-6 — and the anti-inflammatory IL-10, the most probably as a consequence of important inflammation — and CCL2, CCL3 and CXCL10 chemokines, compared to their unprotected sham-vaccinated counterparts **(Figure 7B)**.

Altogether, based on a complete set of virological and immunological data, the LV::S_{FL} vector elicits S_{CoV-2}-specific nAbs and T-cell responses, correlative with substantial level of protection against SARS-CoV-2 infection in two pertinent animal models, and notably upon mucosal i.n. administration.

Discussion

Prophylactic strategies are necessary to control SARS-CoV-2 infection which, 6 months into the pandemic, still continues to spread exponentially without sign of slowing down. It is now demonstrated that primary infection with SARS-CoV-2 in rhesus macaques leads to protective immunity against re-exposure (Chandrashekar et al., 2020). Numerous vaccine candidates, based on naked DNA (Yu et al., 2020) or mRNA, recombinant protein, replicating or non-replicating viral vectors, including adenoviral Ad5 vector (Zhu et al., 2020), or alum-adjuvanted inactivated virus (Gao et al., 2020) are under active development for COVID-19 prevention. Our immunologic rationale for selecting LV to deliver gene encoding S_{CoV-2} antigen is based on the insights obtained on the efficacy of heterologous gene expression *in situ*, as well as the longevity and composite nature of humoral and cell-mediated immunity elicited by this immunization platform. Unique to LV is the ability to transduce proliferating and non-dividing cells such as dendritic cells (Esslinger et al., 2002; Firat et al., 2002; He et al., 2005), thereby LV serves as a powerful vaccination strategy (Beignon et al., 2009; Buffa et al., 2006; Coutant et al., 2012; Gallinaro et al., 2018; Iglesias et al., 2006) to provoke strong and long-lasting adaptive responses (Cousin et al., 2019; Ku et al., Submitted.). Notably, in sharp contrast to many other viral vectors, LV do not suffer from pre-existing immunity in populations, which is linked to their pseudo-typing with the glycoprotein envelope from Vesicular Stomatitis Virus, to which humans are barely exposed. We recently demonstrated that a single injection of a LV expressing Zika envelope provides a rapid and durable protection against Zika infection (Ku et al., 2020). Our recent comprehensive systematic comparison of LV to the gold standard Ad5 immunization vector also documented the superiority of LV to induce multifunctional and central memory T cells in the mouse model, and stronger immunogenicity in outbred rats (Ku et al., Submitted.), underlining the largely adapted properties of LV for vaccinal applications.

Linked to the absence of permissibility of laboratory mice to SARS-CoV-2 replication and the current unavailability of hACE2 transgenic mice in Europe, we set up an *in vivo* transduction murine model in which the hACE2 expression is induced in the respiratory tracts by an i.n. Ad5::hACE2 pretreatment prior to SARS-CoV-2 inoculation. This approach renders mice largely permissive to SARS-CoV-2 replication in the lungs and allows assessment of vaccine or drug efficacy against this virus. This method has also been successfully used to establish the expression of human DPP4 for the study of mouse infection with MERS-CoV (Zhao et al., 2014). Even though the Ad5::hACE2 model may not fully mimic the physiological ACE2 expression profile and thus may not reflect all the aspects of the pathophysiology of SARS-CoV-2 infection, it provides a pertinent model to evaluate *in vivo* the effects of anti-viral drugs, vaccine candidates, various mutations or genetic backgrounds on the SARS-CoV-2 replication. By using a low dose of Ad5::hACE2/mouse, no particular $CD45^+$ cell recruitments

were detectable at day 4 post instillation, indicative of an absence of Ad5-related inflammation before the inoculation of SARS-CoV-2.

We first evaluated the efficacy of LV each encoding one of the variants of S, i.e., full-length, membrane anchored (LV::S_{FL}), S1-S2 ecto-domain, devoid of the transmembrane and C-terminal short internal tail (LV::S1-S2), or S1 alone (LV::S1). Even though a single administration of each of these LV was able to induce high anti-S_{CoV-2} Ab titers, only LV::S_{FL} was able to induce highly functional nAbs. Such single-injection of LV-based vaccine induced a neutralizing activity, which on average was comparable to those found in a cohort of SARS-CoV-2 patients exhibiting mild symptoms. This finding predicted a protective potential of the humoral responses induced by the LV::S_{FL} vector. In parallel, S-specific $CD4^+$ and $CD8^+$ T-cell responses were also observed in the spleen of mice as early as 2 weeks after a single LV::S_{FL} injection, as detected against a single MHC-II- and numerous MHC-I-restricted immunogenic regions that we identified in C57BL/6 ($H\text{-}2^b$) mice.

In the transduced mouse model which allows high rate of SARS-CoV-2 replication, vaccination by a single i.p. administration of 1×10^7 TU of LV::S_{FL}, 6 weeks before the virus inoculation, was sufficient to inhibit the viral replication by ~1 $\log_{10}$. Further boosting via the systemic route did not afford improved protection rate when compared to a single administration. However, priming by systemic route and boosting via mucosal route inhibited efficiently viral replication and avoided lung inflammation. Such protection was correlated with high titers of anti-S_{CoV-2} IgG and a strong neutralization activity in sera. Additional experiments in appropriate KO mice or adoptive immune cell transfer approaches will be necessary to identify the immunological pathways that contribute to disease severity or protection against SARS-CoV-2. Both nAbs and cell-mediated immunity, both very efficaciously induced with the LV-based vaccine candidate, may synergize to blockade infection and viral replication.

Ab-Dependent Enhancement (ADE) of coronavirus entry to the host cells has been evoked as a potential obstacle in vaccination against coronaviruses. With DNA (Yu et al., 2020) or inactivated SARS-CoV-2 virus (Gao et al., 2020) vaccination in macaques, no immunopathological exacerbation has been observed but could not be excluded. Long term observation even after decrease in Ab titer could be necessary to exclude such hypothesis. In the case of MERS-CoV, it has been reported that one particular RBD-specific neutralizing monoclonal Ab (Mersmab1), by mimicking the viral receptor human DPP4 and inducing conformational rearrangements of S_{MERS}, can mediate in vitro ADE of MERS-CoV into the host cells (Wan et al., 2020). We believe that it is difficult to compare the polyclonal Ab response and its paratope repertoire complexity with the singular properties of a monoclonal Ab which cannot be representative of the polyclonal response induced by a vaccine. In addition, very contradictorily, results from the same team reported that a single-dose treatment with a humanized version of Mersmab1 afforded complete protection of a human transgenic mouse model

322 from lethal MERS challenge (Qiu et al., 2016). Therefore, even with an Ab which could facilitate the
323 cell host invasion in vitro in some conditions, not only there is no exacerbation of the infection in vivo,
324 but also there is a notable protection.

325 Substantial degrees of protection against SARS-CoV-2 infection and reduction in the lung
326 inflammation were observed also in *M. auratus* golden hamsters immunized following prime-
327 boost/target regimen with either integrative LV or NILV::S_{FL}. Confirmation of the protection results
328 in this highly sensitive species further favors the LV::S_{FL} vaccine candidate, especially under its non-
329 integrative form, for future introduction into clinical trials.

330 Prophylactic vaccination is the most cost-effective and efficient strategy against infectious diseases
331 in general and against emerging coronaviruses in particular. Our results provide strong evidence that
332 the LV coding for S_{FL} protein of SARS-CoV-2, used via the mucosal route of vaccination, represents
333 a promising vaccine candidate against COVID-19.

334

335

Material and Methods

Construction of transfer pFLAP plasmids coding for S_{FL}, S1-S2, or S1 proteins

A codon-optimized full-length S (1-1273) sequence was amplified from pMK-RQ_S-2019-nCoV and inserted between BamHI and XhoI sites of pFlap-ieCMV-WPREm. Sequences encoding for S1-S2 (1-1211) or S1 (1-681) were amplified by PCR from the pFlap-ieCMV- S_{FL}-WPREm plasmid and sub-cloned into pFlap-ieCMV-WPREm between the BamHI and XhoI restriction sites **(Supplemental Figure 1)**. Each of the PCR products were inserted between the native human ieCMV promoter and a mutated Woodchuck Posttranscriptional Regulatory Element (mWPRE) sequence, where a mutation was introduced to avoid expression of the X protein. Plasmids were amplified in *Escherichia coli* DH5a in Lysogeny Broth supplemented with 50 µg/ml of kanamycin and purified using the NucleoBond Xtra Maxi EF Kit (Macherey Nagel) and resuspended in Tris-EDTA Endotoxin-Free buffer overnight. Plasmid were quantified with a NanoDrop 2000c spectrophotometer (Thermo Scientific), aliquoted and stored at -20°C. Plasmid DNA were verified by enzymatic digestion and by sequencing the region proximal to the transgene insertion sites.

Production and titration of LV

Non-replicative LV were produced in Human Embryonic Kidney (HEK)-293T cells, as previously detailed (Zennou et al., 2000). Briefly, lentiviral particles were produced by transient calcium phosphate co-transfection of HEK293T cells with the vector plasmid pTRIP/sE, a VSV-G Indiana envelope plasmid and an encapsidation plasmid (p8.74 or pD64V for the production of integration-proficient or integration-deficient vectors respectively). Supernatants were harvested at 48h post transfection, clarified by 6-minute centrifugation at 2500 rpm at 4°C. LV were aliquoted and stored at -80°C. Vector titers were determined by transducing 293T cells treated with aphidicolin. The titer, proportional to the efficacy of nuclear gene transfer, is determined as Transduction Unit (TU)/ml by qPCR on total lysates at day 3 post transduction, by use of forward 5'-TGG AGG AGG AGA TAT GAG GG-3' and reverse 5'-CTG CTG CAC TAT ACC AGA CA-3' primers, specific to pFLAP plasmid and forward 5'-TCT CCT CTG ACT TCA ACA GC-3' and reverse 5'-CCC TGC ACT TTT TAA GAG CC-3' primers specific to the host housekeeping gene *gadph* as previously described (Iglesias et al., 2006).

Mouse and hamster studies

Female C57BL/6JRj mice (Janvier, Le Genest Saint Isle, France) were used between the age of 6 and 10 weeks. Male *Mesocricetus auratus* golden hamsters (Janvier, Le Genest Saint Isle, France) were purchased mature, i.e. 80-90 gr weight. At the beginning of the immunization regimen they weigh between 100 and 120 gr. Experimentation on animals was performed in accordance with the European and French guidelines (Directive 86/609/CEE and Decree 87-848 of 19 October 1987) subsequent to

approval by the Institut Pasteur Safety, Animal Care and Use Committee, protocol agreement delivered by local ethical committee (CETEA #DAP20007) and Ministry of High Education and Research APAFIS#24627-2020031117362508 v1. Animals were vaccinated with the indicated TU of LV and sera were collected at various time points post immunization to monitor binding and neutralization activities. Previous to i.m. or i.n. instillations, animals were anesthetized by i.p. injection of a mixture of Ketamine (Imalgene, 50 mg/kg) and Xylazine (Rompun, 50 mg/kg).

SARS-CoV-2 inoculation

Ad5::hACE2-pretreated hamsters or mice were anesthetized by i.p. injection of mixture Ketamine and Xylazine, transferred into a biosafety cabinet 3 where they were inoculated respectively with 0.3 and 1×10^5 $TCID_{50}$ of a SARS-CoV-2 clinical isolate amplified in VeroE6 cells, provided by the Centre National de Réference des Virus Respiratoires, France. The viral inoculum was contained in 20 µl for mice and in 50 µl for hamsters. Animals were then housed in an isolator in BSL3 animal facilities of Institut Pasteur. The organs and fluids recovered from the infected animals, with live SARS-CoV-2 were manipulated following the approved standard operating procedures of the BioSafety Level BSL3 facilities.

Recombinant S_{CoV-2} proteins

Codon-optimized nucleotide fragments encoding a stabilized foldon-trimerized version of the SARS-CoV-2 S ectodomain (a.a. 1 to 1208), the S1 monomer (a.a. 16 to 681) and the RBD subdomain (amino acid 331 to 519) both preceded by a murine IgK leader peptide and followed by an 8xHis Tag were synthetized and cloned into pcDNA™3.1/Zeo$^{(+)}$ expression vector (Thermo Fisher Scientific). Proteins were produced by transient co-transfection of exponentially growing Freestyle™ 293-F suspension cells (Thermo Fisher Scientific, Waltham, MA) using polyethylenimine (PEI)-precipitation method as previously described (Lorin and Mouquet, 2015). Recombinant S_{CoV-2} proteins were purified by affinity chromatography using the Ni Sepharose® Excel Resin according to manufacturer's instructions (Thermo Fisher Scientific). Protein purity was evaluated by in-gel protein silver-staining using Pierce Silver Stain kit (Thermo Fisher Scientific) following SDS-PAGE in reducing and non-reducing conditions using NuPAGE™ 3-8% Tris-Acetate gels (Life Technologies). Purified proteins were dialyzed overnight against PBS using Slide-A-Lyzer® dialysis cassettes (10 kDa MW cut-off, Thermo Fisher Scientific). Protein concentration was determined using the NanoDrop™ One instrument (Thermo Fisher Scientific).

ELISA

Ninety-six-well Nunc Polysorp plates (Nunc, Thermo Scientific) were coated overnight at 4 °C with 100 ng/well of purified S_{CoV-2} proteins in carbonate buffer pH 9.6. The next day, plates were blocked

with carbonate buffer containing 1% BSA for 2 h at 37°C. Wells were then washed with PBS containing 0.05% Tween 20 (PBS-T), 1:100-diluted sera in PBS-T containing 1% BSA and four serial ten-to-ten dilutions were added and incubated during 2h at 37°C. After PBS-T washings, plates were incubated with 1,000-fold diluted peroxydase-conjugated goat anti-mouse IgG (Jackson ImmunoResearch Europe Ltd, Cambridgeshire, United Kingdom) for 1 h. Plates were revealed by adding 100 µl of 3,3',5,5'-tetramethylbenzidine chromogenic substrate (Eurobio Scientific). Following a 30 min incubation, reaction was stopped by adding 100 µl of 2N H2SO4 and optical densities were measured at 450nm/620nm on a PR3100 reader.

nAb Detection

Serial dilutions of heat inactivated sera were assessed for nAbs via an inhibition assay which uses HEK293T cells transduced to stably express human ACE2 and non-replicative S_{CoV-2} pseudo-typed LV particles which harbor the reporter *luciferase firefly* gene, allowing quantitation of the host cell invasion by mimicking fusion step of native SARS-CoV-2 virus (Sterlin et al.). First, 1.5×10^2 TU of S_{CoV-2} pseudo-typed LV were pre-incubated, during 30 min at room temperature, in U-bottom plates, with serial dilutions of each serum in a final volume of 50µl in DMEM-glutamax, completed with 10% heat-inactivated FCS and 100 U/ml penicillin and 100 µg/ml streptomycin. The samples were then transferred into clear-flat-bottom 96-well-black-plates, and each well received 2×10^4 $hACE2^+$ HEK293-T cells, counted in a NucleoCounter NC.200 system (Chemometec, Denmark) contained in 50 µl. After 2 days incubation at 37°C 5% CO_2, the transduction efficiency of $hACE2^+$ HEK293-T cells by pseudo-typed LV particles was determined by measuring the luciferase activity, using a Luciferase Assay System (Promega) on an EnSpire plate reader (PerkinElmer). Results are expressed as percentages of inhibition of luciferase activity compared to the maximum of luciferase activity in the absence of nAbs.

S_{FL} T-cell epitope mapping

In order to map the immuno-dominant epitopes of S_{CoV-2}, peptides spanning the whole S_{FL} (Mimotopes, Australia) were pooled by 25, each containing 15 a.a. residues overlapping by 10 a.a. Peptides were dissolved in DMSO at a concentration of 2 mg/ml and diluted before use at 1 µg/ml (for ELISPOT) or 2–5 µg/mL (for ICS) in α-MEM medium supplemented with 10% FCS, 100 U/ml penicillin and 100 µg/ml streptomycin, 1 x 10-4 M non-essential amino-acids, 1% vol/vol HEPES, 1 x 10-3 M sodium pyruvate and 5×10^{-5} M of β-mercapto-ethanol before use in functional assays. IFN-γ ELISPOT and ICS assays were performed as described previously (Bourgine et al., 2018). For ICS, cells were acquired in an Attune NxT Flow cytometer (ThermoFisher Scientific) and the data were analyzed by FlowJo Software (TreeStar Inc.).

Generation of Ad5 gene transfer vectors and intranasal pretreatment of mice

The Ad5 gene transfer vectors were produced by the use of ViraPower Adenoviral Promoterless Gateway Expression Kit (Thermo Fisher Scientific, France). The sequence containing CMV promoter, BamH1/Xho1 restriction sites and WPRE was PCR amplified from the pTRIPΔU3CMV plasmid, by use of: (i) forward primer, encoding the attB1 in the 5' end, and (ii) reverse primer, encoding both the attB2 and SV40 polyA signal sequence in the 5' end. The attB-PCR product was cloned into the gateway pDORN207 donor vector, via BP Clonase reaction. The *hACE2* was amplified from a plasmid derivative of hACE2-expressing pcDNA3.1[1] (generous gift from Nicolas Escriou) while e*gfp* was amplified from pTRIP-ieCMV-eGFP-WPRE[2]. The amplified PCR products were cloned into the pDORN207 plasmid via the BamH1 and Xho1 restriction sites. To obtain the final Ad5 plasmid, the pDORN207 vector, harboring *hACE2* or *gfp* genes, was further inserted into pAd/PL-DEST™ vector via LR Clonase reaction **(Supplementary Figure 3).**

The Ad5 virions were generated by transfecting the E3-transcomplementing HEK-293A cell line with pAd CMV-GFP-WPRE-SV40 polyA or pAd CMV-hACE2-WPRE-SV40 polyA plasmid followed by subsequent vector amplification, according to the manufacturer's protocol (ViraPower Adenoviral Promoterless Gateway Expression Kit, Thermo Fisher Scientific). The Ad5 particles were purified using Adeno-X rapid Maxi purification kit and concentrated with the Amicon Ultra-4 10k centrifugal filter unit. Vectors were resuspended and stocked à -80°C in PIPES buffer pH 7.5, supplemented with 2.5% glucose. Ad5 were titrated using qRT-PCR protocol, as described by Gallaher et al (Gallaher and Berk, 2013), adapted to HEK-293T cells.

Western blot

Expression of hACE2 in the lungs of Ad5::hACE2-transduced mice was assessed by Western Blotting. One × 10^6 cells from lung homogenate were resolved on 4 – 12 % NuPAGE Bis-Tris protein gels (Thermo Fisher Scientific, France), then transferred onto a nitrocellulose membrane (Biorad, France). The nitrocellulose membrane was blocked in 5 % non-fat milk in PBS-T for 2 hours at room temperature and probed overnight with goat anti-hACE2 primary Ab at 1 µg/mL (AF933, R&D systems). Following three washing intervals of 10 minutes with PBS-T, the membrane was incubated for 1 hour at room temperature with HRP-conjugated anti-goat secondary Ab and HRP-conjugated anti-β-actin (ab197277, Abcam). The membrane was washed with PBS-T thrice before visualization with enhanced chemiluminescence via the super signal west femto maximum sensitivity substrate (ThermoFisher, France) on ChemiDoc XRS+ (Biorad, France). PageRuler Plus prestained protein ladder was used as size reference.

Determination of SARS-CoV-2 viral loads in the lungs

Half of each lung lobes were removed aseptically and frozen at -80°C. Organs were thawed and homogenized for 20 s at 4.0 m/s, using lysing matrix M (MP Biomedical) in 500 µl of ice-cold PBS.

The homogenization was performed in an MP Biomedical Fastprep 24 Tissue Homogenizer. The homogenates were centrifuged 10 min at 2000g for further RNA extraction from the supernatants. Particulate viral RNA was extracted from 70 µl of such supernatants using QIAamp Viral RNA Mini Kit (Qiagen) according to the manufacturer's procedure. Viral load was determined following reverse transcription and real-time TaqMan® PCR essentially as described (Corman et al., 2020), using SuperScriptTM III Platinum One-Step Quantitative RT-PCR System (Invitrogen) and primers and probe (Eurofins) targeting S_{CoV-2} gene as listed in **(Supplemental Table 1)**. In vitro transcribed RNA derived from plasmid pCI/SARS-CoV envelope was synthesized using T7 RiboMAX Express Large Scale RNA production system (Promega), then purified by phenol/chloroform extractions and two successive precipitations with ethanol. RNA concentration was determined by optical density measurement, then RNA was diluted to 10^9 genome equivalents/µL in RNAse-free water containing 100µg/mL tRNA carrier, and stored in single-use aliquots at -80°C. Serial dilutions of this in vitro transcribed RNA were prepared in RNAse-free water containing 10µg/ml tRNA carrier and used to establish a standard curve in each assay. Thermal cycling conditions were: (i) reverse transcription at 55°C for 10 min, (ii) enzyme inactivation at 95°C for 3 min, and (iii) 45 cycles of denaturation/amplification at 95°C for 15 s, 58°C for 30 s. Products were analyzed on an ABI 7500 Fast real-time PCR system (Applied Biosystems).

Cytometric analysis of lung innate immune cells

Lungs from individual mice were treated with collagenase-DNAse-I for a 30-minute incubation at 37°C and homogenized by use of GentleMacs. Cells were filtered through 100 µm-pore filters and centrifuged at 1200 rpm during 8 minutes. Cells were then treated with Red Blood Cell Lysing Buffer (Sigma) and washed twice in PBS. Cells were stained as following. (i) To detect DC, monocytes, alveolar and interstitial macrophages: Near IR Live/Dead (Invitrogen), FcγII/III receptor blocking anti-CD16/CD32 (BD Biosciences), BV605-anti-CD45 (BD Biosciences), PE-anti-CD11b (eBioscience), PE-Cy7-antiCD11c (eBioscience), BV450-anti-CD64 (BD Biosciences), FITC-anti-CD24 (BD Biosciences), BV711-anti-CD103 (BioLegend), AF700-anti-MHC-II (BioLegend), PerCP-Cy5.5-anti-Ly6C (eBioscience) and APC anti-Ly-6G (Miltenyi) mAbs, (ii) to detect neutrophils or eosinophils: Near IR DL (Invitrogen), FcγII/III receptor blocking anti-CD16/CD32 (BD Biosciences), PerCP-Vio700-anti-CD45 (Miltenyi), APC-anti-CD11b (BD Biosciences), PE-Cy7-anti-CD11c (eBioscience), FITC-anti-CD24 (BD Biosciences), AF700-anti-MHC-II (BioLegend), PE-anti-Ly6G (BioLegend), BV421-anti-Siglec-F (BD Biosciences), (iii) to detect mast cells, basophils, NK: Near IR DL (Invitrogen), BV605-anti-CD45 (BD Biosciences), PE-anti-CD11b (eBioscience), eF450-anti-CD11c (eBioscience), PE-Cy7-anti-CD117 (BD Biosciences), APC-anti-FcER1 (BioLegend), AF700-anti-NKp46 (BD Biosciences), FITC-anti-CCR3 (BioLegend), without FcγII/III receptor blocking anti-CD16/CD32. Cells were incubated with appropriate mixtures for 25 minutes at 4°C, washed twice

in PBS containing 3% FCS and then fixed with Paraformaldehyde 4% by an overnight incubation at 4°C. The cells were acquired in on Attune NxT cytometer system (Invitrogen) and data were analyzed by FlowJo software (Treestar, OR, USA).

qRT-PCR Detection of inflammatory cytokines and chemokines in the lungs of the mice and hamsters

Lung samples from mice or hamsters were added to lysing matrix D (MP Biomedical) containing 1 mL of TRIzol reagent and homogenized at 30 s at 6.0 m/s twice using MP Biomedical Fastprep 24 Tissue Homogenizer. Total RNA was extracted using TRIzol reagent (ThermoFisher Scientific, France) according to the manufacturer's procedure. cDNA was synthesized from 4 µg of RNA in the presence of 2.5 µM of oligo(dT) 18 primers, 0.5 mM of deoxyribonucleotides, 2.0 U of RNase Inhibitor and SuperScript IV Reverse Transcriptase (ThermoFisher Scientific, France) in 20 µl reaction. The real-time PCR was performed on QuantStudio™ 7 Flex Real-Time PCR System (ThermoFisher Scientific, France). Reactions were performed in triplicates in a final reaction volume of 10 µl containing 5 µl of iQ™ SYBR® Green Supermix (Biorad, France), 4 µl of cDNA diluted 1:15 in DEPC-water and 0.5 µl of each forward and reverse primers at a final concentration of 0.5 µM **(Supplementary Table 2 and 3)**. The following thermal profile was used: a single cycle of polymerase activation for 3 min at 95°C, followed by 40 amplification cycles of 15 sec at 95°C and 30 sec 60°C (annealing-extension step). Mice β-globin or hamster ribosomal protein L18 (RLP18) was used as an endogenous reference control to normalize differences in the amount of input nucleic acid. The average C_T values were calculated from the technical replicates for relative quantification of target cytokines/chemokines. The differences in the C_T cytokines/chemokines amplicons and the C_T of the endogenous reference control, termed ΔC_T, were calculated to normalize for differences in the quantity of nucleic acid. The ΔC_T of the experimental condition compared relatively to the PBS-immunized individuals using the comparative $\Delta\Delta C_T$ method. The fold change in gene expression was further calculated using $2^{-\Delta\Delta C_T}$.

References

Amanat, F., and F. Krammer. 2020. SARS-CoV-2 Vaccines: Status Report. *Immunity* 52:583-589.

Beignon, A.S., K. Mollier, C. Liard, F. Coutant, S. Munier, J. Riviere, P. Souque, and P. Charneau. 2009. Lentiviral vector-based prime/boost vaccination against AIDS: pilot study shows protection against Simian immunodeficiency virus SIVmac251 challenge in macaques. *J Virol* 83:10963-10974.

Belouzard, S., V.C. Chu, and G.R. Whittaker. 2009. Activation of the SARS coronavirus spike protein via sequential proteolytic cleavage at two distinct sites. *Proc Natl Acad Sci U S A* 106:5871-5876.

Bourgine, M., S. Crabe, Y. Lobaina, G. Guillen, J.C. Aguilar, and M.L. Michel. 2018. Nasal route favors the induction of CD4(+) T cell responses in the liver of HBV-carrier mice immunized with a recombinant hepatitis B surface- and core-based therapeutic vaccine. *Antiviral Res* 153:23-32.

Buffa, V., D.R. Negri, P. Leone, M. Borghi, R. Bona, Z. Michelini, D. Compagnoni, C. Sgadari, B. Ensoli, and A. Cara. 2006. Evaluation of a self-inactivating lentiviral vector expressing simian immunodeficiency virus gag for induction of specific immune responses in vitro and in vivo. *Viral Immunol* 19:690-701.

Chandrashekar, A., J. Liu, A.J. Martinot, K. McMahan, N.B. Mercado, L. Peter, L.H. Tostanoski, J. Yu, Z. Maliga, M. Nekorchuk, K. Busman-Sahay, M. Terry, L.M. Wrijil, S. Ducat, D.R. Martinez, C. Atyeo, S. Fischinger, J.S. Burke, M.D. Slein, L. Pessaint, A. Van Ry, J. Greenhouse, T. Taylor, K. Blade, A. Cook, B. Finneyfrock, R. Brown, E. Teow, J. Velasco, R. Zahn, F. Wegmann, P. Abbink, E.A. Bondzie, G. Dagotto, M.S. Gebre, X. He, C. Jacob-Dolan, N. Kordana, Z. Li, M.A. Lifton, S.H. Mahrokhian, L.F. Maxfield, R. Nityanandam, J.P. Nkolola, A.G. Schmidt, A.D. Miller, R.S. Baric, G. Alter, P.K. Sorger, J.D. Estes, H. Andersen, M.G. Lewis, and D.H. Barouch. 2020. SARS-CoV-2 infection protects against rechallenge in rhesus macaques. *Science. May 2020:eabc4776. doi: 10.1126/science.abc4776. PMID: 32434946.*

Corman, V., T. Bleicker, S. Brünink, and C. Drosten. 2020. Diagnostic detection of 2019-nCoV by real-time RT-PCR. https://www.who.int/docs/default-source/coronaviruse/protocol-v2-1.pdf

Cousin, C., M. Oberkampf, T. Felix, P. Rosenbaum, R. Weil, S. Fabrega, V. Morante, D. Negri, A. Cara, G. Dadaglio, and C. Leclerc. 2019. Persistence of Integrase-Deficient Lentiviral Vectors Correlates with the Induction of STING-Independent CD8(+) T Cell Responses. *Cell Rep* 26:1242-1257 e1247.

Coutant, F., R.Y. Sanchez David, T. Felix, A. Boulay, L. Caleechurn, P. Souque, C. Thouvenot, C. Bourgouin, A.S. Beignon, and P. Charneau. 2012. A nonintegrative lentiviral vector-based vaccine provides long-term sterile protection against malaria. *PLoS One* 7:e48644.

568 Coutard, B., C. Valle, X. de Lamballerie, B. Canard, N.G. Seidah, and E. Decroly. 2020. The spike
569 glycoprotein of the new coronavirus 2019-nCoV contains a furin-like cleavage site absent in
570 CoV of the same clade. *Antiviral Res* 176:104742.
571 Di Nunzio, F., T. Felix, N.J. Arhel, S. Nisole, P. Charneau, and A.S. Beignon. 2012. HIV-derived
572 vectors for therapy and vaccination against HIV. *Vaccine* 30:2499-2509.
573 Esslinger, C., P. Romero, and H.R. MacDonald. 2002. Efficient transduction of dendritic cells and
574 induction of a T-cell response by third-generation lentivectors. *Hum Gene Ther* 13:1091-1100.
575 Firat, H., V. Zennou, F. Garcia-Pons, F. Ginhoux, M. Cochet, O. Danos, F.A. Lemonnier, P. Langlade-
576 Demoyen, and P. Charneau. 2002. Use of a lentiviral flap vector for induction of CTL immunity
577 against melanoma. Perspectives for immunotherapy. *J Gene Med* 4:38-45.
578 Gallaher, S.D., and A.J. Berk. 2013. A rapid Q-PCR titration protocol for adenovirus and helper-
579 dependent adenovirus vectors that produces biologically relevant results. *J Virol Methods*
580 192:28-38.
581 Gallinaro, A., M. Borghi, R. Bona, F. Grasso, L. Calzoletti, L. Palladino, S. Cecchetti, M.F. Vescio,
582 D. Macchia, V. Morante, A. Canitano, N. Temperton, M.R. Castrucci, M. Salvatore, Z.
583 Michelini, A. Cara, and D. Negri. 2018. Integrase Defective Lentiviral Vector as a Vaccine
584 Platform for Delivering Influenza Antigens. *Front Immunol* 9:171.
585 Gao, Q., L. Bao, H. Mao, L. Wang, K. Xu, M. Yang, Y. Li, L. Zhu, N. Wang, Z. Lv, H. Gao, X. Ge,
586 B. Kan, Y. Hu, J. Liu, F. Cai, D. Jiang, Y. Yin, C. Qin, J. Li, X. Gong, X. Lou, W. Shi, D. Wu,
587 H. Zhang, L. Zhu, W. Deng, Y. Li, J. Lu, C. Li, X. Wang, W. Yin, Y. Zhang, and C. Qin. 2020.
588 Rapid development of an inactivated vaccine candidate for SARS-CoV-2. *Science. 2020 Jul*
589 *3;369(6499):77-81. doi: 10.1126/science.abc1932. Epub 2020 May 6.PMID: 32376603.*
590 Guo, Y.R., Q.D. Cao, Z.S. Hong, Y.Y. Tan, S.D. Chen, H.J. Jin, K.S. Tan, D.Y. Wang, and Y. Yan.
591 2020. The origin, transmission and clinical therapies on coronavirus disease 2019 (COVID-19)
592 outbreak - an update on the status. *Mil Med Res* 7:11.
593 He, Y., J. Zhang, Z. Mi, P. Robbins, and L.D. Falo, Jr. 2005. Immunization with lentiviral vector-
594 transduced dendritic cells induces strong and long-lasting T cell responses and therapeutic
595 immunity. *J Immunol* 174:3808-3817.
596 Hu, B., A. Tai, and P. Wang. 2011. Immunization delivered by lentiviral vectors for cancer and
597 infectious diseases. *Immunol Rev* 239:45-61.
598 Iglesias, M.C., M.P. Frenkiel, K. Mollier, P. Souque, P. Despres, and P. Charneau. 2006. A single
599 immunization with a minute dose of a lentiviral vector-based vaccine is highly effective at
600 eliciting protective humoral immunity against West Nile virus. *J Gene Med* 8:265-274.
601 Ku, M.W., F. Anna, F. Souque, S. Petres, M. Prot, E. Simon-Loriere, P. Charneau, and M. Bourgine.
602 2020. A Single Dose of NILV-Based Vaccine Provides Rapid and Durable Protection against

Zika Virus. *Mol Ther. 2020 May 20;S1525-0016(20)30250-1. doi: 10.1016/j.ymthe.2020.05.016.*

Ku, M.W., P. Authié, P. Souque, M. Bourgine, M. Romano, P. Charneau, and L. Majlessi. Submitted. High-Quality Memory T Cells by Programmed Antigen Expression in Dendritic Cells Induced by Lentiviral Vector.

Lai, A.L., J.K. Millet, S. Daniel, J.H. Freed, and G.R. Whittaker. 2017. The SARS-CoV Fusion Peptide Forms an Extended Bipartite Fusion Platform that Perturbs Membrane Order in a Calcium-Dependent Manner. *J Mol Biol* 429:3875-3892.

Lorin, V., and H. Mouquet. 2015. Efficient generation of human IgA monoclonal antibodies. *J Immunol Methods* 422:102-110.

Qiu, H., S. Sun, H. Xiao, J. Feng, Y. Guo, W. Tai, Y. Wang, L. Du, G. Zhao, and Y. Zhou. 2016. Single-dose treatment with a humanized neutralizing antibody affords full protection of a human transgenic mouse model from lethal Middle East respiratory syndrome (MERS)-coronavirus infection. *Antiviral Res* 132:141-148.

Rosenberg, S.A., Y. Zhai, J.C. Yang, D.J. Schwartzentruber, P. Hwu, F.M. Marincola, S.L. Topalian, N.P. Restifo, C.A. Seipp, J.H. Einhorn, B. Roberts, and D.E. White. 1998. Immunizing patients with metastatic melanoma using recombinant adenoviruses encoding MART-1 or gp100 melanoma antigens. *J Natl Cancer Inst* 90:1894-1900.

Schirmbeck, R., J. Reimann, S. Kochanek, and F. Kreppel. 2008. The immunogenicity of adenovirus vectors limits the multispecificity of CD8 T-cell responses to vector-encoded transgenic antigens. *Mol Ther* 16:1609-1616.

Sia, S.F., L.M. Yan, A.W.H. Chin, K. Fung, K.T. Choy, A.Y.L. Wong, P. Kaewpreedee, R. Perera, L.L.M. Poon, J.M. Nicholls, M. Peiris, and H.L. Yen. 2020. Pathogenesis and transmission of SARS-CoV-2 in golden hamsters. *Nature. 2020 May 14. doi: 10.1038/s41586-020-2342-5. Online ahead of print.PMID: 32408338.*

Sterlin, D., A. Mathian, M. Miyara, A. Mohr, F. Anna, L. Claër, P. Quentric, J. Fadlallah, P. Ghillani, C. Gunn, R. Hockett, S. Mudumba, A. Guihot, C. Luyt, J. Mayaux, A. Beurton, S. Fourati, J. Lacorte, H. Yssel, C. Parizot, K. Dorgham, P. Charneau, Z. Amoura, and G. Gorochov. IgA dominates the early neutralizing antibody response to SARS-CoV-2. https://www.medrxiv.org/content/10.1101/2020.06.10.20126532v1:

Vabret, N., G.J. Britton, C. Gruber, S. Hegde, J. Kim, M. Kuksin, R. Levantovsky, L. Malle, A. Moreira, M.D. Park, L. Pia, E. Risson, M. Saffern, B. Salome, M. Esai Selvan, M.P. Spindler, J. Tan, V. van der Heide, J.K. Gregory, K. Alexandropoulos, N. Bhardwaj, B.D. Brown, B. Greenbaum, Z.H. Gumus, D. Homann, A. Horowitz, A.O. Kamphorst, M.A. Curotto de Lafaille, S. Mehandru, M. Merad, R.M. Samstein, and P. Sinai Immunology Review. 2020. Immunology of COVID-19: Current State of the Science. *Immunity* 52:910-941.

639 Walls, A.C., Y.J. Park, M.A. Tortorici, A. Wall, A.T. McGuire, and D. Veesler. 2020. Structure,
640 Function, and Antigenicity of the SARS-CoV-2 Spike Glycoprotein. *Cell* 181:281-292 e286.
641 Wan, Y., J. Shang, S. Sun, W. Tai, J. Chen, Q. Geng, L. He, Y. Chen, J. Wu, Z. Shi, Y. Zhou, L. Du,
642 and F. Li. 2020. Molecular Mechanism for Antibody-Dependent Enhancement of Coronavirus
643 Entry. *J Virol* 94:
644 Wang, Q., Y. Qiu, J.Y. Li, Z.J. Zhou, C.H. Liao, and X.Y. Ge. 2020. A Unique Protease Cleavage Site
645 Predicted in the Spike Protein of the Novel Pneumonia Coronavirus (2019-nCoV) Potentially
646 Related to Viral Transmissibility. *Virol Sin. 2020 Jun;35(3):337-339. doi: 10.1007/s12250-*
647 *020-00212-7. Epub 2020 Mar 20.*
648 Yu, J., L.H. Tostanoski, L. Peter, N.B. Mercado, K. McMahan, S.H. Mahrokhian, J.P. Nkolola, J. Liu,
649 Z. Li, A. Chandrashekar, D.R. Martinez, C. Loos, C. Atyeo, S. Fischinger, J.S. Burke, M.D.
650 Slein, Y. Chen, A. Zuiani, N.L. FJ, M. Travers, S. Habibi, L. Pessaint, A. Van Ry, K. Blade, R.
651 Brown, A. Cook, B. Finneyfrock, A. Dodson, E. Teow, J. Velasco, R. Zahn, F. Wegmann, E.A.
652 Bondzie, G. Dagotto, M.S. Gebre, X. He, C. Jacob-Dolan, M. Kirilova, N. Kordana, Z. Lin,
653 L.F. Maxfield, F. Nampanya, R. Nityanandam, J.D. Ventura, H. Wan, Y. Cai, B. Chen, A.G.
654 Schmidt, D.R. Wesemann, R.S. Baric, G. Alter, H. Andersen, M.G. Lewis, and D.H. Barouch.
655 2020. DNA vaccine protection against SARS-CoV-2 in rhesus macaques. *Science. 2020 May*
656 *20;eabc6284. doi: 10.1126/science.abc6284. PMID: 32434945.*
657 Zennou, V., C. Petit, D. Guetard, U. Nerhbass, L. Montagnier, and P. Charneau. 2000. HIV-1 genome
658 nuclear import is mediated by a central DNA flap. *Cell* 101:173-185.
659 Zhao, J., K. Li, C. Wohlford-Lenane, S.S. Agnihothram, C. Fett, J. Zhao, M.J. Gale, Jr., R.S. Baric, L.
660 Enjuanes, T. Gallagher, P.B. McCray, Jr., and S. Perlman. 2014. Rapid generation of a mouse
661 model for Middle East respiratory syndrome. *Proc Natl Acad Sci U S A* 111:4970-4975.
662 Zhu, F.C., Y.H. Li, X.H. Guan, L.H. Hou, W.J. Wang, J.X. Li, S.P. Wu, B.S. Wang, Z. Wang, L. Wang,
663 S.Y. Jia, H.D. Jiang, L. Wang, T. Jiang, Y. Hu, J.B. Gou, S.B. Xu, J.J. Xu, X.W. Wang, W.
664 Wang, and W. Chen. 2020. Safety, tolerability, and immunogenicity of a recombinant
665 adenovirus type-5 vectored COVID-19 vaccine: a dose-escalation, open-label, non-
666 randomised, first-in-human trial. *Lancet. 2020 Jun 13;395(10240):1845-1854. doi:*
667 *10.1016/S0140-6736(20)31208-3. Epub 2020 May 22. P.*

668

669

Figure Legend

Figure 1. Induction of S_{CoV-2}-specific antibody responses by LV. (A) Schematic representation of 3 forms of S_{CoV-2} protein (S_{FL}, S1-S2 and S1) encoded by LV injected to mice. RBD, S1/S2 and S2' cleavage sites, Fusion Peptide (FP), TransMembrane (TM) and short internal tail (T) are indicated. **(B)** Dynamic of S_{CoV-2}-specific Ab response following LV immunization. C57BL/6 mice (n = 4/group) were injected i.p. with 1×10^7 TU of LV::S_{FL}, LV::S1-S2, LV::S1 or, LV::GFP as a negative control. Sera were collected at 1, 3, 4 and 6 weeks post immunization. Anti-S_{CoV-2} IgG responses were evaluated by ELISA and expressed as mean endpoint dilution titers. **(C)** Neutralization capacity of S_{CoV-2}-specific antibodies induced by LV::S_{FL} immunization. Mouse sera were evaluated in a sero-neutralization assay to determine 50% effective concentration (EC50) neutralizing titers. (D) Correlation between the Ab titers and neutralization activity in various experimental groups. NS: not significant. **(E)** Head-to-head comparison at a 1:40 dilution between mouse sera taken at weeks 3 or 4 after immunization and a cohort of mildly symptomatic people living in Crépy en Valois, Ile de France. These patients did not seek medical attention and recovered from COVID-19. Results are expressed as Mean ± SEM percentages of inhibition of luciferase activity.

Figure 2. Induction of T-cell responses by LV::S_{FL}. Naive C57BL/6 mice (n = 5) were immunized i.p. with 1×10^7 TU of LV::S_{FL}. **(A)** Splenocytes collected 2 weeks later were subjected to an IFN-γ ELISPOT using pools of peptides spanning the entire S_{CoV-2} (1-1273 a.a.). SFC = Spot-Forming Cells. **(B)** Deconvolution of the peptide pools by intracellular IFN-γ staining in 5 individual mice. IFN-γ-secreting $CD4^+$ or $CD8^+$ T cells were detected after stimulation with individual peptides from positive pools. Percentages of S_{CoV2}-specific IFN-γ-producing cells versus total $CD4^+$ or $CD8^+$ T cells are shown as color map. ND = not done.

Figure 3. In vivo transduction of mouse respiratory tract cells by an Ad5::hACE2 pretreatment, allowing permissibility to SARS-CoV-2 replication. (A) Detection of hACE2 expression by RT-PCR in HEK293 T cells transduced with Ad5::hACE2 at 2 days post transduction. **(B)** hACE2 protein detection by Western Blot in lung cell extracts recovered at day 4 after i.n. instillation of Ad5::hACE2 or empty Ad5 to C57BL/6 mice (n = 2/group). **(C)** GFP expression in the lung cells prepared at day 4 after i.n. instillation of Ad5::GFP or PBS into C57BL/6 mice, as assessed by flow cytometry in the $CD45^+$ hematopoietic or $EpCam^+$ epithelial cells. **(D)** Lung viral loads in mice pretreated with Ad5::hACE2, control empty Ad5 or PBS followed by i.n. inoculation of 1×10^5 $TCID_{50}$ of SARS-CoV-2 4 days later. Viral loads quantification by qPCR in the lung homogenates at 2, 4 or 7 dpi. Limit of detection is shown by a brown line **(E)** Percentages of $CD45^+$ cells, and **(F)** SARS-CoV-2 viral loads in the lungs at day 4 after i.n. instillation of various doses of Ad5::hACE2.

Figure 4. Protective potential of LV::S_{FL} immunization against SARS-CoV-2 in mice. (A) Time line of vaccination by a single injection of LV followed by Ad5::hACE2 pretreatment and SARS-CoV-

2 challenge. **(B)** Lung viral loads in unvaccinated mice, LV::S_{FL}- or sham-immunized mice, at 3 dpi post challenge. **(C)** Time line of the prime-boost strategy based on LV, followed by Ad5::hACE2 pretreatment and SARS-CoV-2 challenge. **(D)** Titers of S_{CoV-2}-specific IgG, able to bind to S_{CoV-2}, as quantitated by ELISA in the sera of C57BL/6 mice primed i.p. at week 0 and boosted i.p. or i.n. at week 3. Titers are determined as mean endpoint dilution. *** $P<0.001$; **** $P<0.0001$. ns, not significant. **(E)**. Lung viral loads at 3 dpi in mice primed (i.p.) and boosted (i.p. or i.n.) with LV::S_{FL}. Sham-vaccinated received an empty LV. Statistical significance of the differences in the viral loads was evaluated by two tailed unpaired t test; * = $p<0.0139$, *** = $p<0.0088$.

Figure 5. Inflammation mediators in the lungs of unvaccinated or vaccinated and protected mice. (A) Gating strategy applied to total lung cells to quantitate the key innate immune subsets. **(B)** Percentages of each innate immune subset versus total lung $CD45^+$ cells at 3 dpi in mice sham-vaccinated or vaccinated with LV::S_{FL}, following various prime-boost regimen compared to non-infected (NI) controls which only received PBS. All the mice have been pretreated with Ad5::hACE-2, 4 days prior to SARS-CoV-2 inoculation. **(C)** Relative $\log_2$ fold change in cytokines and chemokines expression of mice sham-vaccinated or vaccinated with LV::S_{FL}, following various prime-boost regimen at 3 dpi.

Figure 6. LV::S_{FL} immunization against SARS-CoV-2 in hamsters. (A) Time line of the LV::S_{FL} prime-boost/target immunization regimen and SARS-CoV-2 challenge in hamsters. (n = 6/group). Sham-vaccinated received an empty LV. **(B)** Dynamic of S_{CoV-2}-specific Ab response following LV immunization. Sera were collected from sham- or LV-vaccinated hamsters at 3, 5 (pre-boost), and 6 (post-boost) weeks after the prime injection. Anti-S_{CoV-2} IgG responses were evaluated by ELISA and expressed as mean endpoint dilution titers. **(C)** Post boost/target EC50 neutralizing titers, determined in the hamsters' sera after boost, and as compared to the sera from a cohort of symptomatic (S), pauci-symptomatic (PS), symptomatic (S) or healthy COVID-19 contacts (H) humans **(D)** Weight follow-up in hamsters, either sham-vaccinated or vaccinated with diverse doses of LV::S_{FL}.

Figure 7. Protective potential of LV::S_{FL} immunization against SARS-CoV-2 in hamsters. Animals are those detailed in the Figure 6. **(A)** Lung viral loads at 2 or 4 dpi with SARS-CoV-2 in LV::S_{FL}-vaccinated hamsters. Statistical significance of the differences in the viral loads was evaluated by two tailed unpaired t test; * = $p<0.0402$, **** = $p<0.0001$. **(B)** Relative $\log_2$ fold changes in cytokines and chemokines expression of LV::S_{FL}-vaccinated and protected hamsters versus unprotected sham-vaccinated individuals, as determined at 4 dpi by qRT-PCR in the total lung homogenates. And normalized versus untreated controls. Statistical significance of the differences in cytokines and chemokines level was evaluated by one-way ANOVA; * = $p<0.05$, ** = $p<0.01$.

739

Author Contribution

Study concept and design: MWK, MB, FA, AM, NE, LM, PC, acquisition of data: MWK, MB, PA, JL, KN, BV, PS, FA, AM, LM, construction and production of LV and technical support: PA, FM, AN, FN, CB, PS, analysis and interpretation of data: MWK, MB, PA, JL, KN, FA, AM, NE, LM, PC, recombinant S proteins: HM, drafting of the manuscript: MWK, MB, LM.

Declaration of Interests

PC is the founder and CSO of TheraVectys. Other authors declare no competing interests.

Acknowledgments

The authors are grateful to Cyril Planchais for the preparation of recombinant Tri-S, S1 and RBD proteins and Damien Batalie for technical assistance in determination of viral loads.

This work is also supported by grants from Institut Pasteur, TheraVectys and Agence Nationale de la Recherche (ANR) HuMoCID.

Figure 1

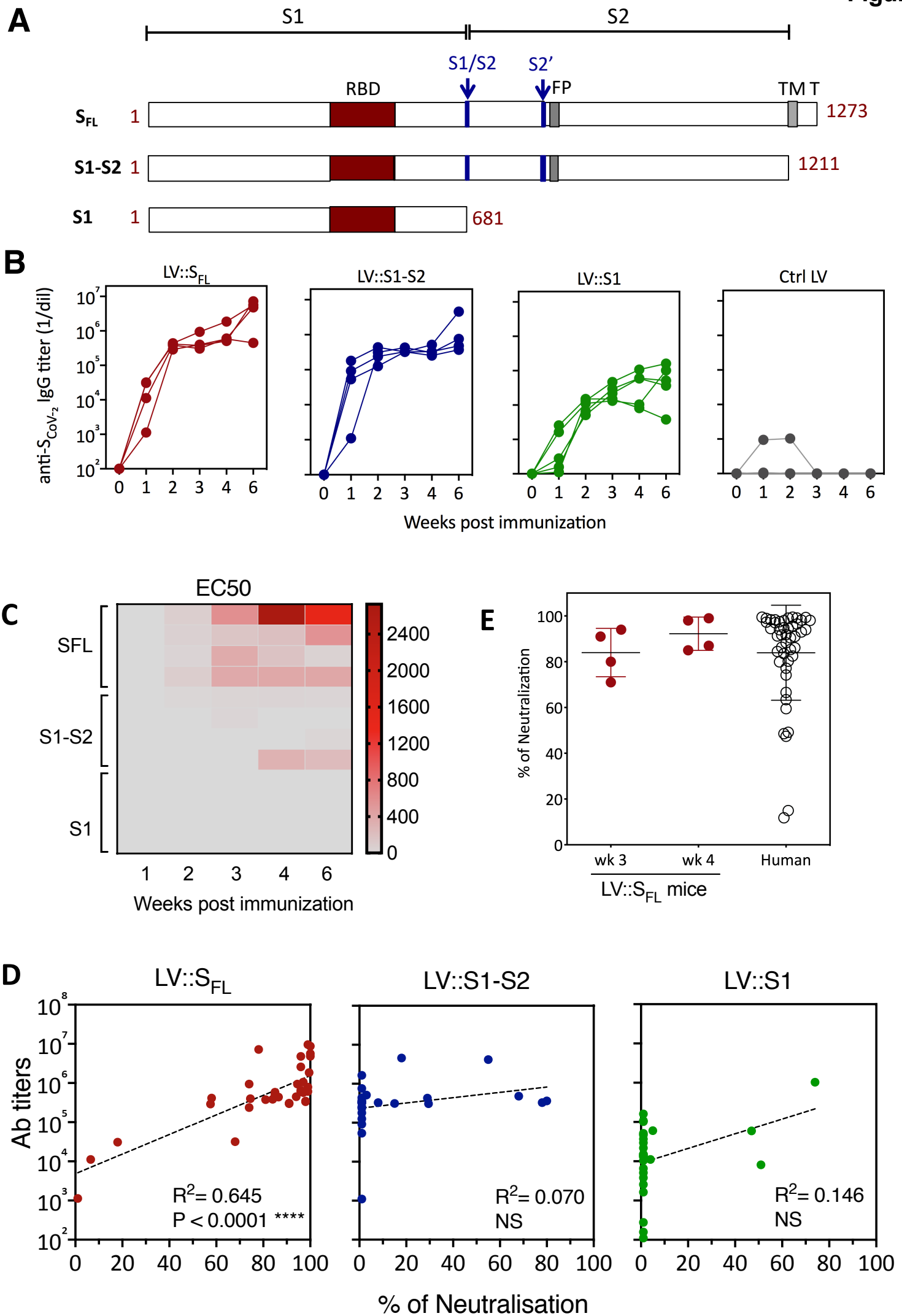

Figure 2

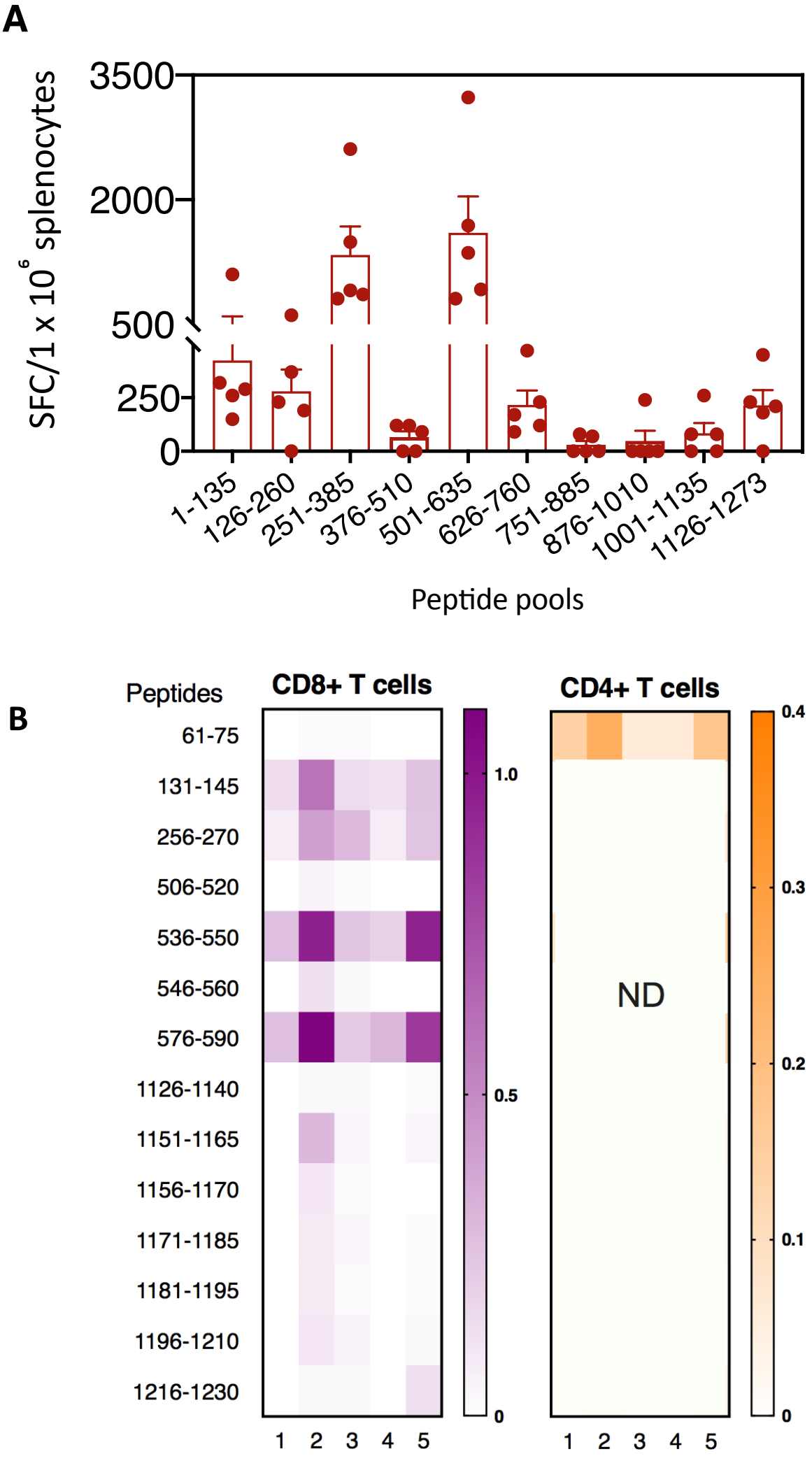

Figure 3

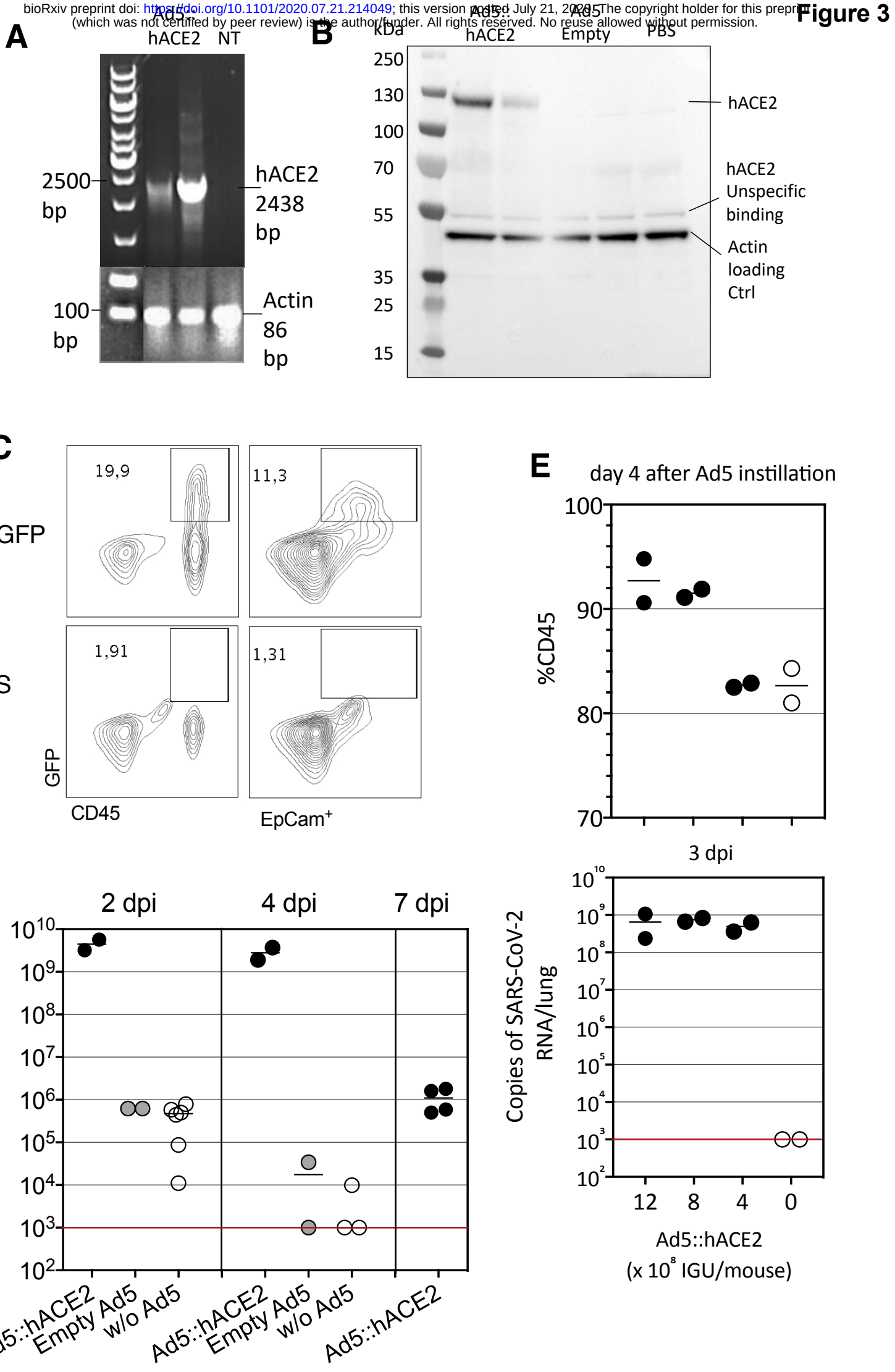

Figure 4

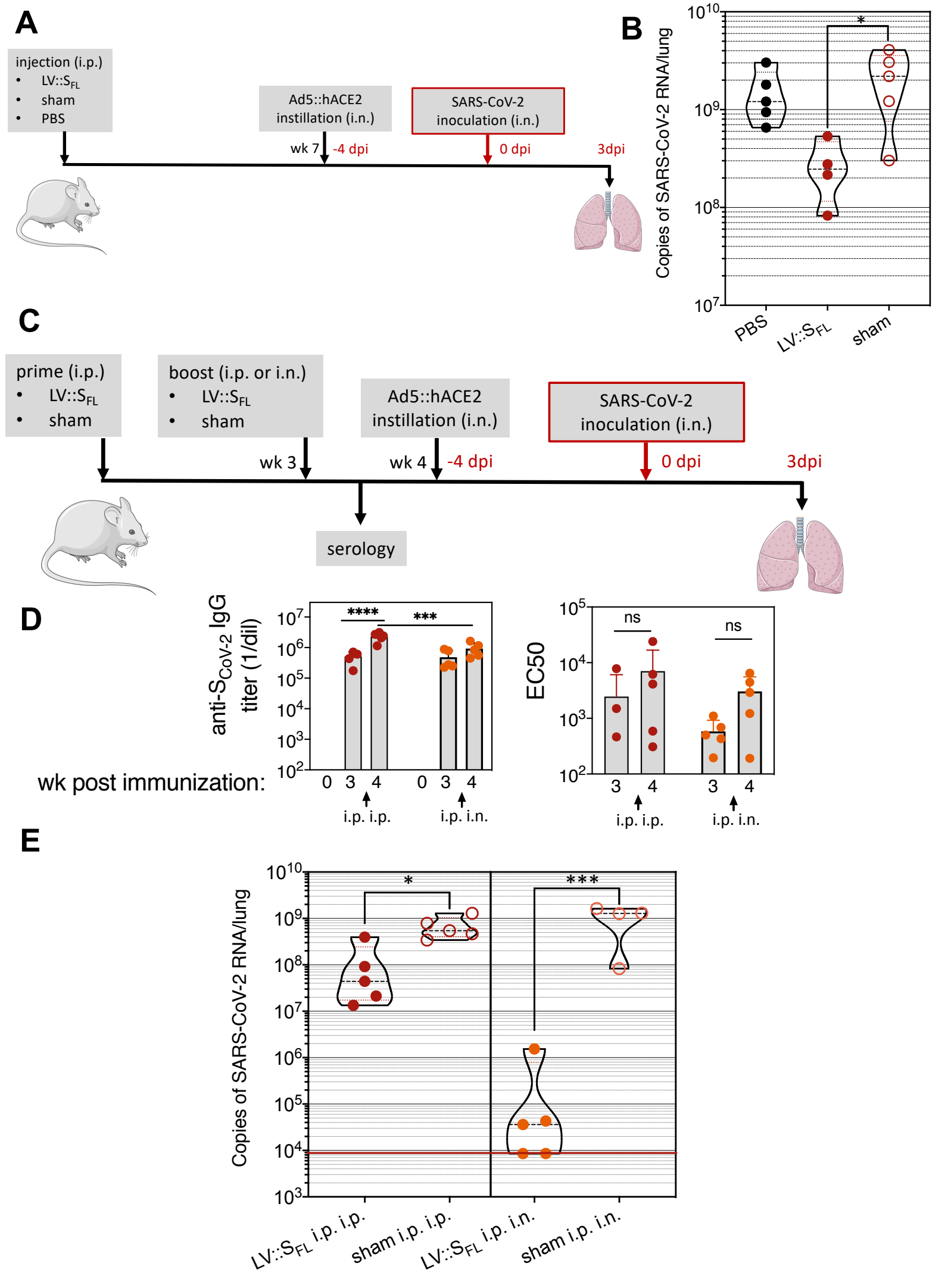

Figure 5

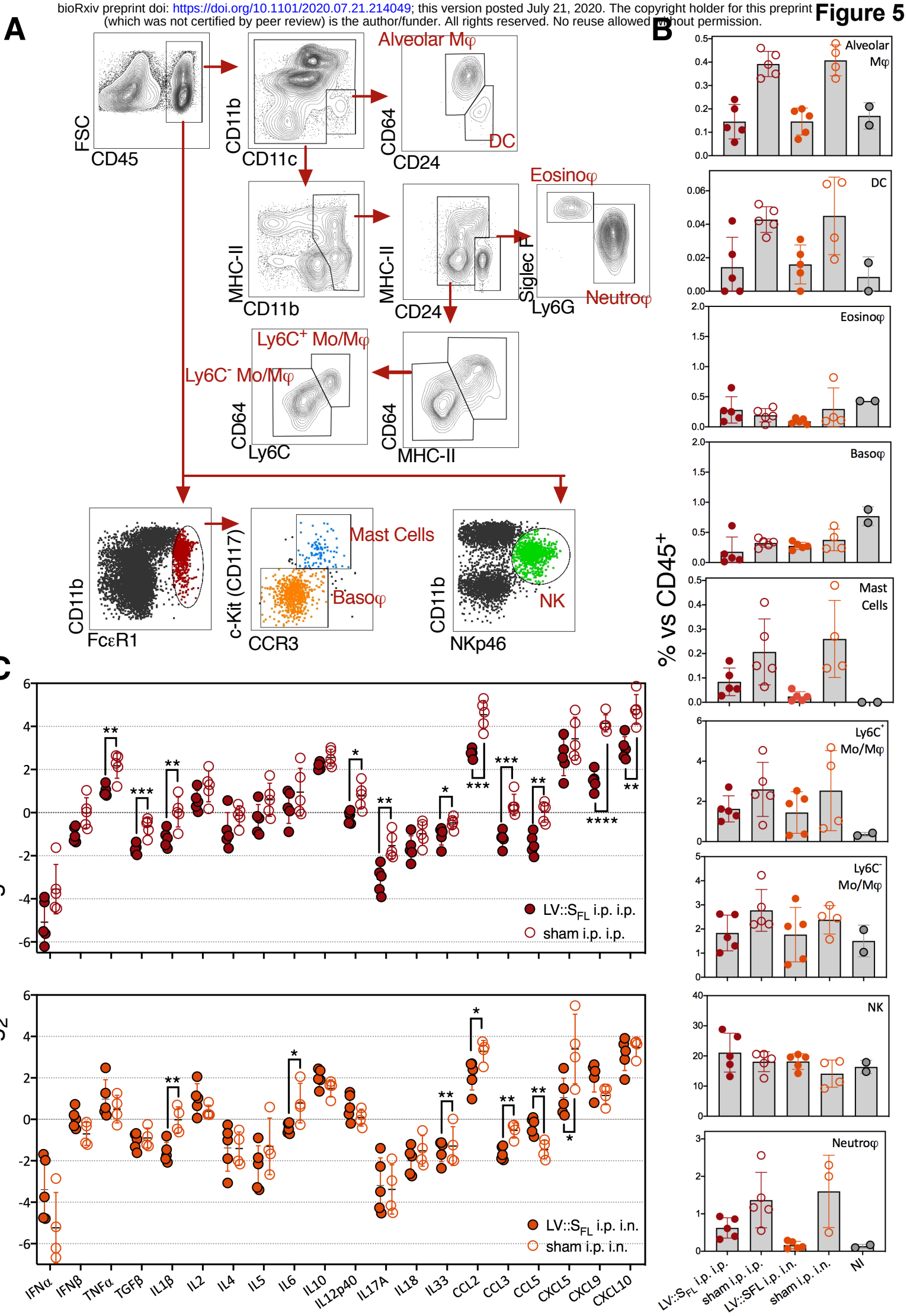

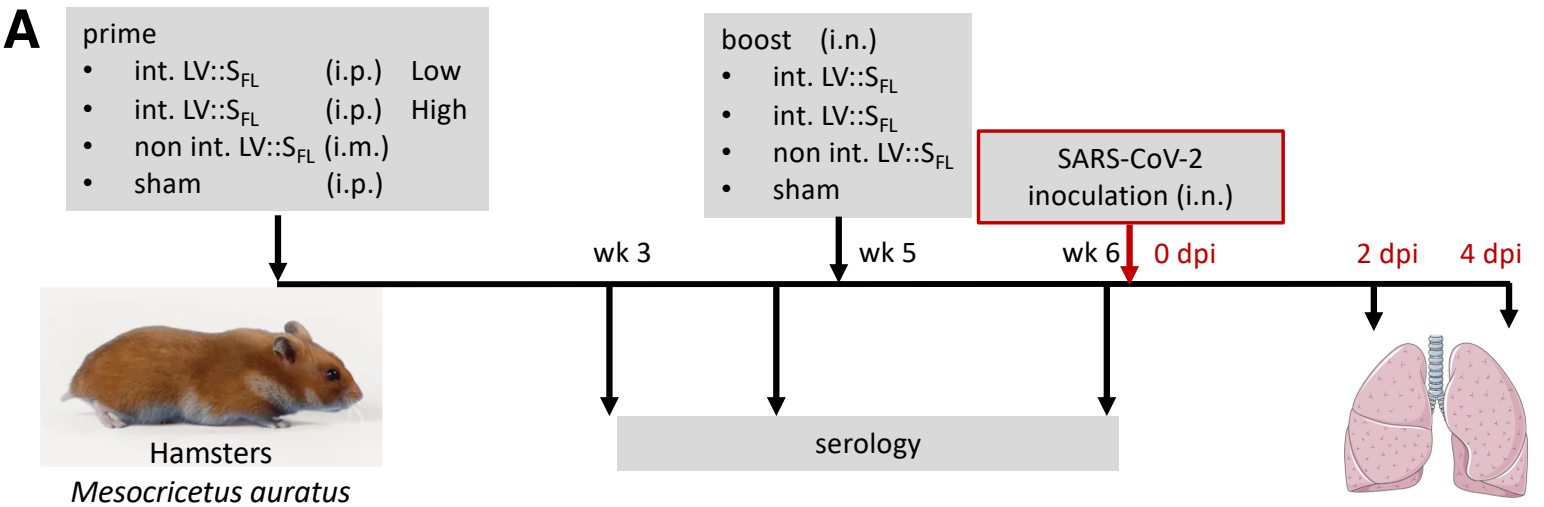
A
prime
• int. LV::S$_{FL}$ (i.p.) Low
• int. LV::S$_{FL}$ (i.p.) High
• non int. LV::S$_{FL}$ (i.m.)
• sham (i.p.)
boost (i.n.)
• int. LV::S$_{FL}$
• int. LV::S$_{FL}$
• non int. LV::S$_{FL}$
• sham
SARS-CoV-2 inoculation (i.n.)
wk 3
wk 5
wk 6
0 dpi
2 dpi
4 dpi
serology
Hamsters
Mesocricetus auratus

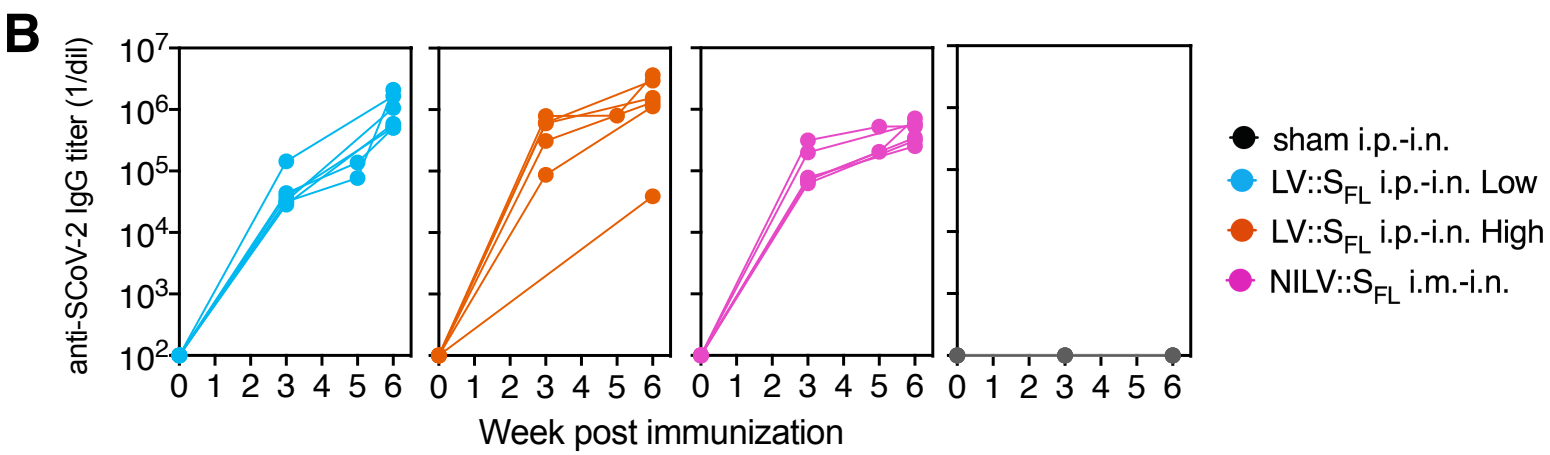
B
anti-SCoV-2 IgG titer (1/dil)
Week post immunization
sham i.p.-i.n.
LV::S$_{FL}$ i.p.-i.n. Low
LV::S$_{FL}$ i.p.-i.n. High
NILV::S$_{FL}$ i.m.-i.n.

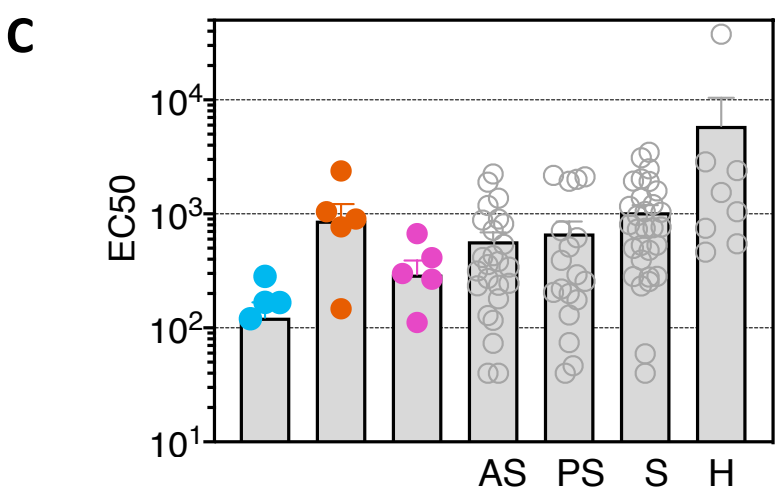
C
EC50
AS
PS
S
H

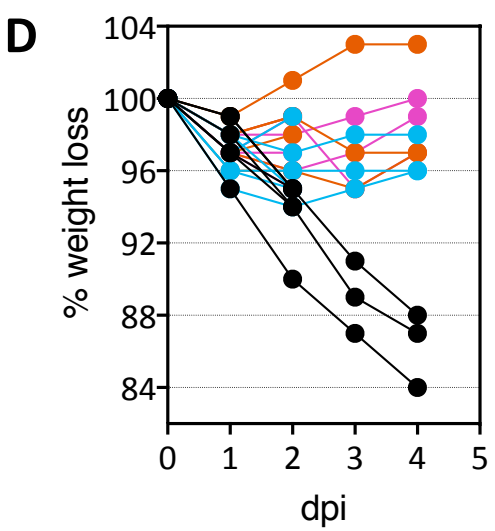
D
% weight loss
dpi

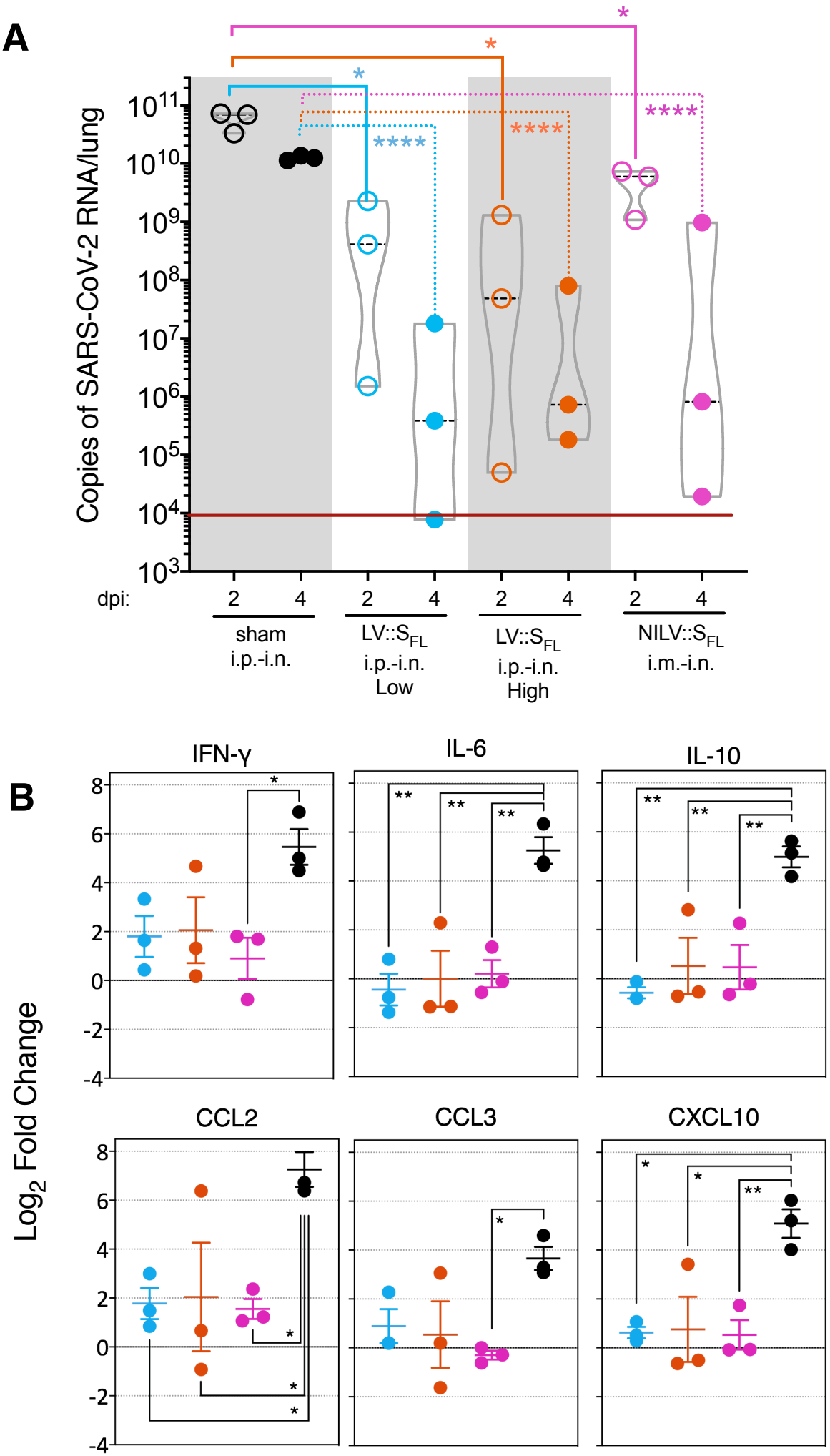
A
Copies of SARS-CoV-2 RNA/lung
10^{11}
10^{10}
10^{9}
10^{8}
10^{7}
10^{6}
10^{5}
10^{4}
10^{3}
dpi:
2
4
sham
i.p.-i.n.
LV::S_{FL}
i.p.-i.n.
Low
LV::S_{FL}
i.p.-i.n.
High
NILV::S_{FL}
i.m.-i.n.
B
Log$_2$ Fold Change
IFN-γ
IL-6
IL-10
CCL2
CCL3
CXCL10